

## Structural design of a wide-ridge mid-wave infrared quantum cascade laser based on a supersymmetric waveguide

DU Shu-Hao<sup>1</sup>, ZHENG Xian-Tong<sup>1\*</sup>, JIA Han<sup>2</sup>, CUI Jin-Tao<sup>2</sup>, ZHANG Shi-Ya<sup>2</sup>,  
LIU Yuan<sup>1</sup>, FENG Yu-Lin<sup>1</sup>, ZHANG Chun-Qian<sup>3</sup>, LIU Ming<sup>4</sup>, ZHANG Dong-Liang<sup>4\*</sup>

- (1. Laboratory of Optoelectronic Materials and Devices, School of Instrumental Science and Optoelectronic Engineering, Beijing Information Science and Technology University, Beijing 100192, China;
2. Key Laboratory of Optoelectronic Test Technology and Instrumentation, Ministry of Education of China, Beijing Information Science and Technology University, Beijing 100016, China;
3. School of Applied Science, Beijing Information Science and Technology University, Beijing 100192, China;
4. The 11th Research Institute of China Electronics Technology Group Corporation, Beijing 100015, China)

**Abstract:** In the process of power scaling large-area Quantum Cascade Lasers (QCLs), challenges such as degradation of beam quality and emission of multilobed far-field modes are frequently encountered. These issues become particularly pronounced with an increase in ridge width, resulting in multimode problems. To tackle this, an innovative multi ridge waveguide structure based on the principle of supersymmetry (SUSY) was proposed. This structure comprises a wider main waveguide in the center and two narrower auxiliary waveguides on either side. The high-order modes of the main waveguide are coupled with the modes of the auxiliary waveguides through mode-matching design, and the optical loss of the auxiliary waveguides suppresses these modes, thereby achieving fundamental mode lasing of the wider main waveguide. This paper employs the finite difference eigenmode (FDE) method to perform detailed structural modeling and simulation optimization of the 4.6  $\mu\text{m}$  wavelength quantum cascade laser, successfully achieving a single transverse mode QCL with a ridge width of 10  $\mu\text{m}$ . In comparison to the traditional single-mode QCL (with a ridge width of about 5  $\mu\text{m}$ ), the MRW structure has the potential to increase the gain area of the laser by 100%. This offers a novel design concept and methodology for enhancing the single-mode luminous power of mid-infrared quantum cascade lasers, which is of considerable significance.

**Key words:** quantum cascade laser, mode competition, supersymmetry, mid-infrared, auxiliary waveguides

## 基于超对称波导的宽脊中波量子级联激光器结构设计

杜舒豪<sup>1</sup>, 郑显通<sup>1\*</sup>, 贾涵<sup>2</sup>, 崔锦涛<sup>2</sup>, 张诗雅<sup>2</sup>, 柳渊<sup>1</sup>, 冯玉林<sup>1</sup>, 张春倩<sup>3</sup>,  
刘铭<sup>4</sup>, 张东亮<sup>4\*</sup>

- (1. 北京信息科技大学 仪器科学与光电工程学院 光电材料与器件实验室, 北京 100192;
2. 北京信息科技大学 光电测量技术与仪器仪表教育部重点实验室, 北京 100016;
3. 北京信息科技大学 理学院, 北京 100192
4. 中国电子科技集团公司第十一研究所, 北京 100015)

**摘要:** 在大面积量子级联激光器功率扩展过程中, 经常遇到光束质量下降、多叶远场模式发射等挑战。这些问题随着脊宽的增加而变得尤为突出, 最终导致多模问题。针对这一问题, 提出了一种基于超对称原理的创新多脊波导结构。该结构由中间较宽的主波导和两边较窄的辅助波导组成。通过模式匹配设计将主波导的高阶模式与辅助波导的模式耦合, 辅助波导的光损耗抑制这些高阶模式, 从而实现较宽主波导的基模激光。

**Received date:** 2024-09-15, **revised date:** 2024-12-06

**收稿日期:** 2024-09-15, **修回日期:** 2024-12-06

**Foundation item:** Supported by the National Natural Science Foundation of China (62105039)

**Biography:** DU Shu-Hao (1999—), male, Xiangyang, Hubei, China, master. Research area includes high power mid-wave infrared quantum cascade lasers. E-mail: dushh22@outlook.com

\* **Corresponding authors:** E-mail: zxt1001@bistu.edu.cn, zdllzu2007@163.com

本文采用有限差分特征模方法对 4.6  $\mu\text{m}$  波长量子级联激光器进行了详细的结构建模和仿真优化, 成功实现了脊宽 10  $\mu\text{m}$  的单横模 QCL。与传统单模 QCL(脊宽约 5  $\mu\text{m}$ ) 相比, MRW 结构有可能使激光器的增益面积提高 100%, 为提升中红外量子级联激光器单模发光功率提供了一种新颖的设计理念和办法, 具有重要意义。

**关键词:** 量子级联激光器; 模式竞争; 超对称; 中红外; 辅助波导

**中图分类号:** TN252

**文献标识码:** A

## Introduction

High-power quantum cascade lasers are widely employed in fields such as directional infrared countermeasures, long-distance detection of hazardous chemicals, infrared laser guidance, and long-distance free-space optical communication<sup>[1-4]</sup>. To maintain the single spatial mode operation of Mid Wave Infrared (MWIR) QCL, a Ridge Waveguide (RW) structure is typically adopted, which suppresses high-order modes by reducing the ridge width<sup>[5]</sup>. However, the narrow ridge width reduces the gain area of the laser while suppressing high-order modes, greatly limiting the maximum output power of the device. Consequently, to solve this problem, additional structures need to be introduced into the device to ensure that the active area is increased while avoiding the occurrence of high-order modes<sup>[6]</sup>. Existing methods for implementing transverse mode filtering include oblique-angle resonators<sup>[7]</sup>, oscillating power amplifiers<sup>[4]</sup>, and photonic crystal resonators in surface-emitting lasers<sup>[8-10]</sup>, and so on.

In recent years, a new Parity-Time (PT) symmetric design method has been established, which utilizes the concept of selective breaking of parity-time symmetry<sup>[9]</sup>. This method can help lasers achieve better mode control and thus achieve single-mode lasing in transverse multimode micro-rings<sup>[11]</sup>. To further increase power, the principle of supersymmetry (SUSY) has also been introduced into the design of coupled laser arrays<sup>[12-13]</sup>. These designs have shown great application prospects in micro-ring resonator arrays and strip waveguide arrays<sup>[14]</sup>. This paper designs a mid-infrared quantum cascade laser with a MRW structure based on the SUSY principle for the first time, aiming to achieve high-power single transverse mode output of MWIR-QCL. This work serves as a valuable reference for the structural optimization and performance enhancement of high-power mid-infrared quantum cascade lasers.

## 1 Principle

Based on the idea of supersymmetry and PT symmetry, this paper adds additional optical structure to traditional ridge waveguide laser to suppress the higher-order modes while increasing the ridge width. The design principle is as follows. The core idea of the unbroken SUSY optical architecture is to construct a superpaired system of a known optical system<sup>[15-17]</sup>, by localizing the fundamental mode in the original waveguide (array) and coupling the remaining high-order modes to the super-paired waveguide. In optical systems, PT symmetry mandates that the complex refractive index distribution fulfills  $n(x) = n^*(-x)$ <sup>[18]</sup>, indicating that the refractive index is

even symmetric, while the distribution of gain and loss should be odd symmetric. However, the distribution of gain and loss is usually not strictly odd in practical devices. But as long as the distribution is asymmetric, quasi-PT symmetry can still be achieved<sup>[19]</sup>. Specifically, artificially introducing loss in the superpaired waveguide is used to magnify the laser gain threshold difference between the fundamental mode and the higher-order modes, thereby achieving fundamental mode output. According to the coupled-mode theory, the coupling strength between modes is determined by the coupling coefficient, phase mismatch (the difference in the real part of the propagation constant  $\text{Re}\{\beta\}$ ), and the difference in gain and loss. The effective coupling will split the coupled mode into symmetric and antisymmetric supermode pairs<sup>[20]</sup>.

The cross-section of the MRW structure proposed in this study is shown in Figure 1 (a). This structure includes a main waveguide in the middle position and a pair of auxiliary waveguides with losses on both sides. As shown in the figure, the widths of the three ridge waveguides are described as  $W_L$  (left waveguide width),  $W_M$  (main waveguide width), and  $W_R$  (right waveguide width), respectively. The two trench widths  $W_E$  between the three ridges are set to be equal. The role of the auxiliary waveguides on both sides (superpaired waveguide system) is to realize the unbroken SUSY architecture, that is, through the MRW structure design, its mode propagation constants  $\beta$  match the propagation constants of the relevant modes in the main waveguide except the fundamental mode, and other modes in the main waveguide except the fundamental mode will be split into supermode pairs through coupling. The design principles of each waveguide is shown in Figure 1 (b)<sup>[11]</sup>. In this design, the widened main waveguide allows support for high-order modes, while the auxiliary waveguide is designed to both support coupling with the high-order modes of the main waveguide (select TM1 of the main waveguide to couple with TM0 of the left waveguide, and TM2 couples with TM1 of the right waveguide), and can also filter out unnecessary high-order modes by introducing additional optical losses. The additional optical loss imposed in the auxiliary waveguide results in greater optical losses for high-order supermodes, thereby increasing their lasing thresholds. At the same time, the fundamental mode will maintain the lowest lasing threshold without being affected, thereby becoming the laser mode in mode competition<sup>[21]</sup>, ensuring that the device has a larger fundamental mode lasing area and higher output power than traditional RW MWIR-QCL.

This study uses the MODE solver in Lumerical to perform mode analysis on the device under study, and by

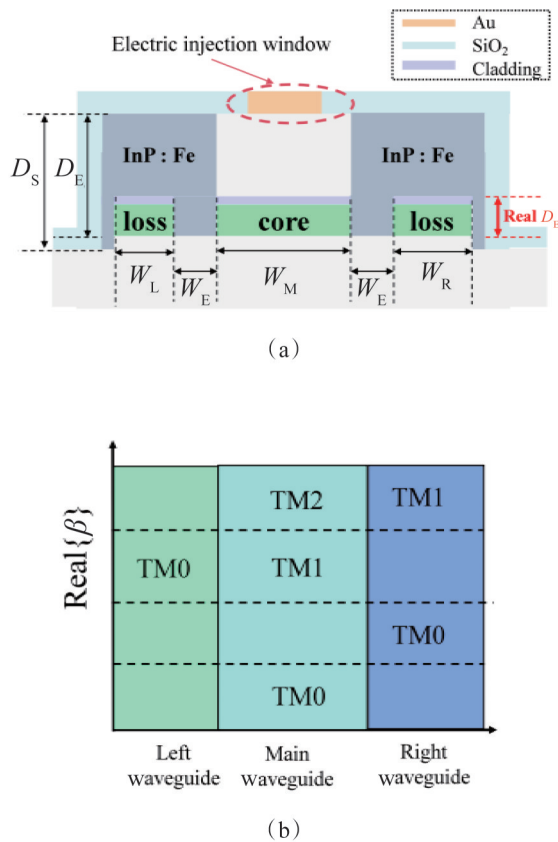


Fig. 1 Schematic structure of the MRW device structure and principle: (a) Cross-section of the MRW; (b) Design principle of mode coupling

图1 MRW 器件结构和原理示意图: (a) 器件横截面; (b) 主波导与左、右辅助波导的模式耦合设计原则

setting the imaginary part  $n_i$  of the complex refractive index  $n = n_r + in_i$  to impose additional losses. According to  $n_i = -\alpha\lambda/4\pi$  ( $\alpha$  is positive for gain,  $\alpha$  is negative for loss),  $n_i$  is calculated based on the material composition. To enhance mode selection, it is assumed that a uniform loss of  $20 \text{ cm}^{-1}$  is applied in the superpaired auxiliary waveguide. The longitudinal material structure and refractive index parameters of this device have been reported detailedly in our previous research<sup>[22]</sup>, and the working wavelength is  $4.6 \mu\text{m}$ . Concurrently, the transverse magnetic mode (TM) polarization is dominant in QCL, and only the TM mode is analyzed in the simulation. Compared with the SUSY laser array, the MRW structure proposed in this paper is simpler in design and practice. Furthermore, the strategy proposed in this study has no specific requirements for the epitaxial structure, is compatible with the manufacturing technology of traditional RW MWIR-QCL, and is more likely to achieve large-scale and low-cost production. Next, the specific structural design will be discussed to explain the basic mechanisms and design points.

## 2 Results and discussions

A simulation was conducted to determine the width of each waveguide based on the relationship between the ridge width and the propagation constant of a single ridge

waveguide, and the results are shown in Figure 2. Based on the coupled-mode theory, the coupling of laser modes in the resonator is closely related to the real part of the propagation constant. When the width of the main waveguide is fixed at  $10 \mu\text{m}$ , it can be seen that it supports three modes: TM0, TM1, and TM2. According to the mode coupling principle in Figure 1 (b), the narrower waveguide widths that match the propagation constants of main waveguide TM1 and TM2 can be found. These widths are subsequently used as the structural parameters of the auxiliary waveguides. As shown in Figure 2, the width of the left auxiliary waveguide corresponding to TM1 ( $W_L^1 = 4.9 \mu\text{m}$ ) has been determined, while the right auxiliary waveguide corresponding to TM2 has two widths sum  $W_R^1$  and  $W_R^2$ . It can be seen that the waveguide width corresponding to  $W_R^1$  is pretty narrow. Considering the fabrication technology limitations, the right auxiliary waveguide width has been selected to be the wider one, namely  $6.5 \mu\text{m}$ . Since other structural parameters have not yet been determined, the width of the auxiliary waveguide at this time is a rough initial value, and more accurate widths of the auxiliary waveguides will be selected next.

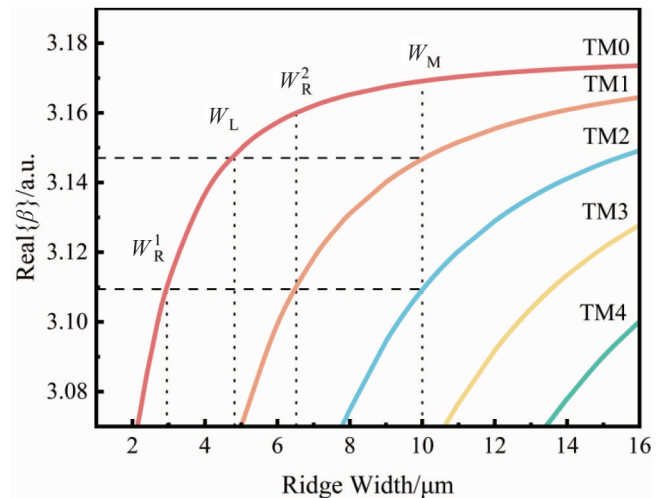


Fig. 2 The propagation constant real part of TM modes in QCL as a function of ridge width

图2 QCL中TM模的传播常数实部和脊宽的关系

$\Delta\text{Loss1}$  is the mode loss difference between the fundamental mode with the lowest loss and the high-order mode with the second lowest loss in the existing modes of the main waveguide. The larger this value, the stronger the mode recognition ability and the better the selectivity for the fundamental mode.  $\Delta\text{Loss2}$  is the mode loss difference between TM1 of the main waveguide and TM0 of the left auxiliary waveguide. It represents the coupling efficiency of the first-order mode of the main waveguide and the fundamental mode of the left auxiliary waveguide. The smaller this value, the greater the mode overlap and the higher the coupling efficiency. Similarly,  $\Delta\text{Loss3}$  is the mode loss difference between TM2 of the main waveguide and TM1 of the right auxiliary wave-

guide. It represents the coupling efficiency of the second-order mode of the main waveguide and the first-order mode of the right auxiliary waveguide. At the same time, considering that when the trench depth is shallow, the laser may exhibit the characteristics of a super wide single ridge laser (more than 20  $\mu\text{m}$ ), a reasonable trench depth needs to be considered. According to the design principle in Figure 1 (b), there should only be 6 transverse magnetic modes in this MRW QCL. Firstly, the width of the main waveguide was fixed at 10  $\mu\text{m}$ , as illustrated in Figure 2, with a selected  $W_L$  of 4.9  $\mu\text{m}$  and  $W_R$  of 6.5  $\mu\text{m}$ . The relationship between the number of modes that can exist in the laser and the etching depth ( $D_E$ ) was then scanned. The outcome is illustrated in Figure 3, which demonstrates that upon reaching a depth of 4.6  $\mu\text{m}$ , it was observed that the laser exhibited only six distinct transverse modes.

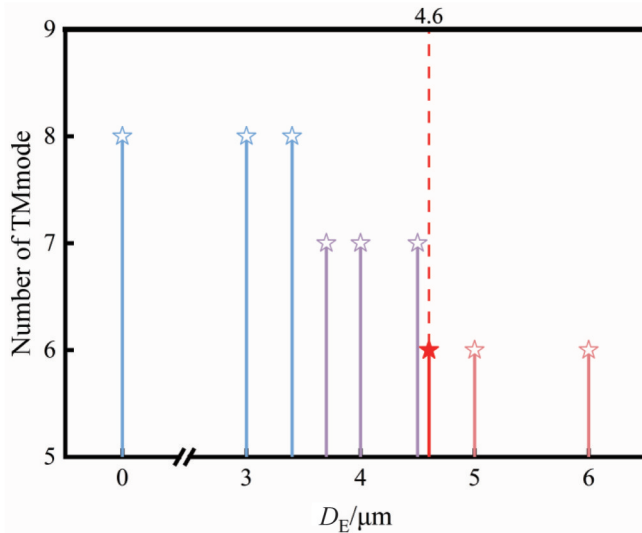
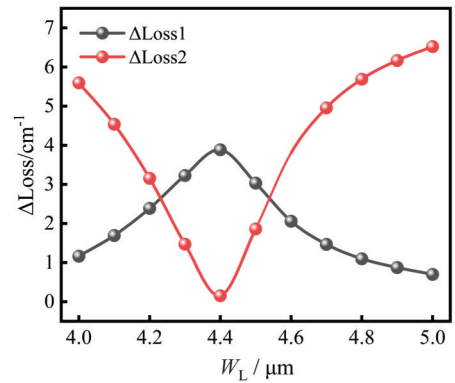
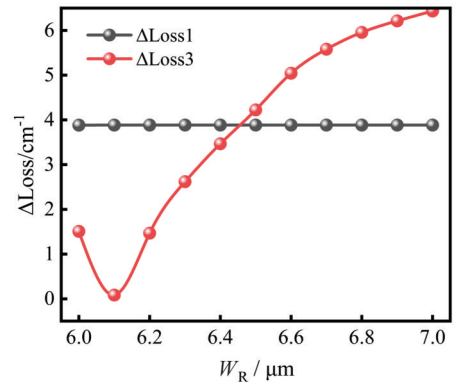


Fig. 3 The number of modes in the laser at different trench etching depths (The geometric parameters are  $W_M = 10 \mu\text{m}$ ,  $W_L = 4.9 \mu\text{m}$ ,  $W_R = 6.5 \mu\text{m}$ , respectively.)  
图3 不同沟槽刻蚀深度下激光器的模式数,对应的结构参数分别为  $W_M = 10 \mu\text{m}$ ,  $W_L = 4.9 \mu\text{m}$ ,  $W_R = 6.5 \mu\text{m}$

To achieve fundamental mode lasing, the selection principle of MRW structural parameters is to ensure that the fundamental mode selectivity in the main waveguide is the strongest while the coupling efficiencies of high-order modes are the highest, that is, the fundamental mode is constrained in the main waveguide, and the energy of high-order modes is mainly concentrated in the lossy auxiliary waveguide. Figure 4 shows the effect of ridge width on coupling results. For the left auxiliary waveguide,  $\Delta\text{Loss1}$  should be the largest, and  $\Delta\text{Loss2}$  should be the smallest. Similarly, for the width of the right auxiliary waveguide, the same principle should be followed, that is,  $\Delta\text{Loss1}$  should be the largest, and  $\Delta\text{Loss3}$  should be the smallest. According to the scanning results, it is finally selected that the optimal matching widths of the left auxiliary waveguide and the right auxiliary waveguide are 4.4  $\mu\text{m}$  and 6.1  $\mu\text{m}$ , respectively.



(a)



(b)

Fig. 4 Effect of the ridge width on the coupling results: (a) Loss margin of modes as a function of the left ridge width; (b) Loss margin of modes as a function of the left ridge width  
图4 脊宽对耦合结果的影响:(a)左侧波导脊宽对MRW结构模式损耗差值的影响;(b)右侧波导脊宽对MRW结构模式损耗差值的影响

Figure 5 (a) shows the impact of trench etching depth  $D_E$  on the structure. It can be seen that the low-order supermodes are robust to the etching depth, while the high-order supermodes are highly dependent on the etching depth. For the selection of structural parameters, in addition to the above principles, the feasibility of the process must also be taken into account. Considering the scanning results in Figure 5 (a),  $D_E = 5 \mu\text{m}$  is selected. In the simulation process, it was found that the sidewall etching depth  $D_s$  also has an important impact on the MRW structure, as shown in Figure 5 (b). The sidewalls of conventional RW QCLs are typically etched to the junction of the core layer and the lower cladding layer, with a depth of approximately 5  $\mu\text{m}$ . This paper selects 5  $\mu\text{m}$  as the starting point for sidewall etching and finally determines the optimal  $D_s$  is 5.7  $\mu\text{m}$ . In addition, the etching width has an extremely important impact on the coupling efficiency. If the etching width is too wide, it will form a discrete laser array, which can prevent the laser's transverse mode from coupling through the MRW structure. On the other hand, if the width is too narrow, it can create excessive strain during the etching process, making it difficult to fabricate the device. Figure 5 (c)

shows the role of trench width  $W_E$ . It can be observed that as the etching width increases,  $\Delta\text{Loss1}$  decreases while  $\Delta\text{Loss2}$  increases, which indicates that the loss of the TM1 mode of the main waveguide decreases, that is, the high-order modes do not couple with the modes existing in the auxiliary waveguides, then the mode loss difference between TM1 and TM0 of the main waveguide decreases, and at the same time, the mode loss difference between TM1 of the main waveguide and TM0 of the left auxiliary waveguide increases, manifesting as a significant decrease in the mode selectivity of the laser and a significant decrease in coupling efficiency, which is consistent with the expected conjecture. Given the feasibility of the etching process, a  $W_E$  of  $1.5 \mu\text{m}$  can be selected. And now the aspect ratio of trenches is  $5/1.5$ , it's still hard in manufacturing, therefore we used InP doped Fe to fill the trench and replace the up-cladding layers InP above the auxiliary waveguides whose total thickness is  $3 \mu\text{m}$ . Because InP doped Fe and the up-cladding layer InP have the same refractive index parameter, therefore the simulation results are the same as before. So the real  $D_E$  is  $2 \mu\text{m}$  (the red mark on the right side of Figure 1 (a) shows the Real  $D_E$ ) In the meantime, the aspect ratio of the trenches has been reduced to  $2/1.5$  which will greatly reduce the difficulty of manufacturing.

After two modes are coupled, they split into pairs of supermodes, resulting in a significant change in the distribution of field strength (energy) compared to the uncoupled modes. Using the optimized structural parameters mentioned earlier, the energy distribution of the modes before and after coupling is calculated. Figures 6 to 8 display the changes in the modes of the main waveguide before and after coupling. Figures (a) and (b) show the mode distributions of the independent single-ridge structure laser with their ridge widths corresponding to the ridge widths of the main waveguide and auxiliary waveguide in the MRW structure respectively ( $10/6.1/4.4 \mu\text{m}$ ); c and d correspond to the mode distribution of the MRW laser, with the corresponding structural parameters being  $W_M = 10 \mu\text{m}$ ,  $W_L = 4.4 \mu\text{m}$ ,  $W_R = 6.1 \mu\text{m}$ ,  $D_E = 5 \mu\text{m}$ , and  $D_S = 5.7 \mu\text{m}$ , respectively.

Figure 7(a) shows the uncoupled mode TM1 of the  $10 \mu\text{m}$  single ridge laser. According to the design principle in Figure 1(b), the fundamental mode of the left auxiliary waveguide (with a ridge width of  $4.4 \mu\text{m}$ , shown in Figure 7(b)) matches it. After coupling in the MRW, these two matching modes split into a supermode pair, as shown in Figures 7(c) and 7(d). Numerical simulation results indicate that the energy ratio of the core area of the  $10 \mu\text{m}$  single ridge laser is 0.78 before coupling, while the energy ratio of the core area of the main waveguide in the MRW after coupling is 0.31 (Figure 7(c)) and 0.33 (Figure 7(d)).

Figure 8(a) shows the uncoupled mode TM2 of the  $10 \mu\text{m}$  single ridge laser. As per the design principle illustrated in Figure 1(b), the high-order mode of the right auxiliary waveguide (with a ridge width of  $6.1 \mu\text{m}$ , shown in Figure 8(b)) matches it. Similarly, these two matching modes split into a supermode pair after cou-

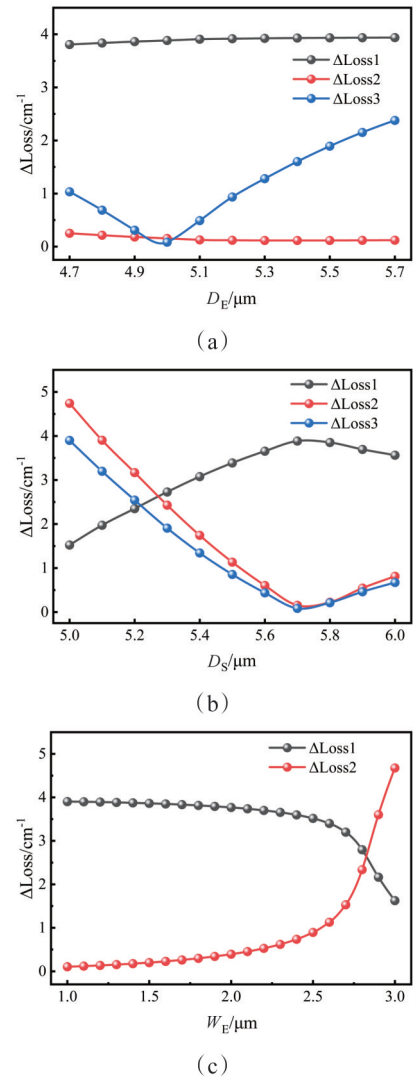


Fig. 5 Effect of different parameters on loss margin of modes in MRW structure: (a) Loss margin of modes as a function of trench etch depth; (b) Loss margin of modes as a function of etch side depth; (c) Loss margin of modes as a function of trench etch depth  
图5 不同参数对MRW结构模式损耗差值的影响:(a)沟槽深度对MRW结构模式损耗差值的影响;(b)侧壁深度对MRW结构模式损耗差值的影响;(c)沟槽宽度对MRW结构模式损耗差值的影响

pling in the MRW, as shown in Figures 8(c) and 8(d). Based on numerical simulation results, the energy ratio of the core area of the  $10 \mu\text{m}$  single ridge laser is 0.77 before coupling, and the energy ratio of the core area of the main waveguide in the MRW structure after coupling is 0.34 (Figure 8(c)) and 0.36 (Figure 8(d)). It is evident that, in the main waveguide, all high-order modes, except for the fundamental mode, are coupled. Furthermore, the energy of the high-order modes in the main waveguide is concentrated in the auxiliary waveguide, indicating that MRW has a strong ability to filter out high-order modes.

Figure 9 illustrates the correlation between the real part of the effective refractive index and the loss of modes in both the MRW laser and the traditional  $10 \mu\text{m}$  wide

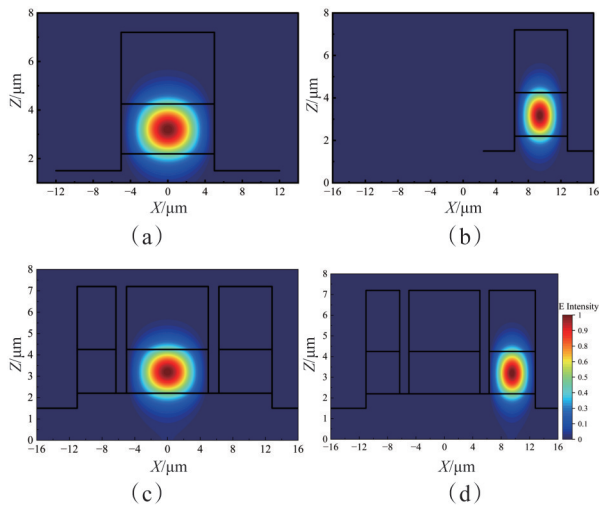


Fig. 6 Field strength distribution of the fundamental modes in the laser: (a) Field strength component of the fundamental mode supported by the  $10\ \mu\text{m}$  independent single ridge laser; (b) Field strength component of the fundamental mode supported by the  $6.1\ \mu\text{m}$  independent single ridge laser; (c) Field strength component of the fundamental mode in the main waveguide of MRW laser; (d) Field strength component of the fundamental mode in right auxiliary waveguide of MRW laser

图6 激光器中基模的场强分布:(a)  $10\ \mu\text{m}$  独立单脊激光器基模的场强分布;(b)  $6.1\ \mu\text{m}$  独立单脊激光器基模的场强分布;(c) MRW 激光器主波导中基模的场强分布;(d) MRW 激光器右辅助波导中基模的场强分布

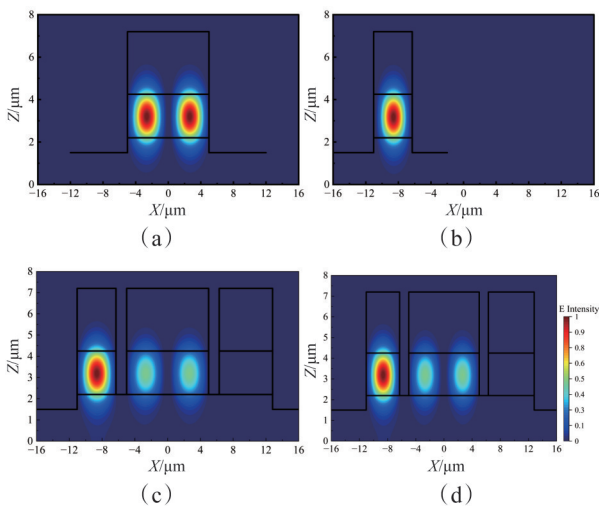


Fig. 7 Field strength distribution of high-order mode in the laser: (a) Field strength component of 1st order mode supported by the  $10\ \mu\text{m}$  independent single ridge laser; (b) Field strength component of the fundamental mode supported by the  $4.4\ \mu\text{m}$  independent single ridge laser; (c) Field strength component of the first order supermode in main waveguide of MRW laser; (d) Field strength component of first order supermode in the left auxiliary waveguide of MRW laser

图7 激光器中高阶模式的场强分布:(a)  $10\ \mu\text{m}$  独立单脊激光器一阶模的场强分布;(b)  $4.4\ \mu\text{m}$  独立单脊激光器基模的场强分布;(c) MRW 激光器主波导一阶超模的场强分布;(d) MRW 激光器中左辅助波导一阶超模的场强分布

single RW laser. The loss difference between the fundamental mode and the lowest loss mode in the high-order

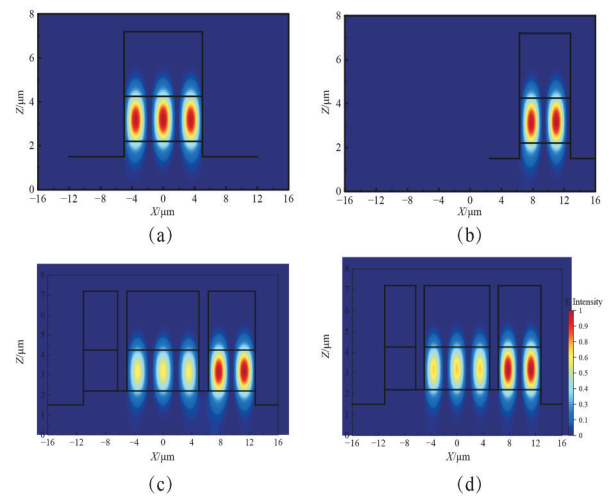


Fig. 8 Field strength distribution of high-order mode in the laser: (a) Field strength component of 2nd order mode supported by the  $10\ \mu\text{m}$  independent single ridge laser; (b) Field strength component of 1st order mode supported by the  $6.1\ \mu\text{m}$  independent single ridge laser; (c) Field strength component of the second order supermode in the main waveguide of MRW laser; (d) Field strength component of second order supermode in the right auxiliary waveguide of MRW laser

图8 激光器中高阶模式的场强分布:(a)  $10\ \mu\text{m}$  独立单脊激光器二阶模的场强分布;(b)  $6.1\ \mu\text{m}$  独立单脊激光器一阶模的场强分布;(c) MRW 激光器主波导二阶超模的场强分布;(d) MRW 激光器中右辅助波导二阶超模的场强分布

modes represents the mode distinction of the laser. The traditional RW laser has a very small mode loss difference of approximately  $0.11\ \text{cm}^{-1}$ , indicating a low ability to distinguish between modes. This can result in all three modes reaching the threshold simultaneously, leading to multi-mode lasing, mode competition, hopping, and a decrease in beam quality. In contrast, the MRW structure utilizes super-paired auxiliary waveguides to couple and split all modes in the main waveguide, except for the fundamental mode, into high-loss supermodes. By introducing additional losses to filter out high-order modes, a stable single-mode laser can be achieved. The mode discrimination in MRW is significantly higher reaching  $3.9\ \text{cm}^{-1}$ .

### 3 Conclusions

In this study, a new wide-ridge MRW MWIR-QCL waveguide structure was designed based on the unbroken SUSY principle. The structure comprises a primary waveguide situated in the center, accompanied by a pair of lossy auxiliary waveguides on either side, and the side-wall etching depth in this structure is about  $0.7\ \mu\text{m}$  deeper than the trench depth. By coupling the high-order modes of the main waveguide with the modes of the auxiliary waveguide, the lasing thresholds of the main waveguide high-order modes were raised, achieving the fundamental mode lasing of the device. Compared with array structures or taper waveguide structures, this structure is relatively simple and straightforward to fabricate. Additionally, compared with the conventional  $5\ \mu\text{m}$  wide single ridge waveguide MWIR-QCL, this design realizes a

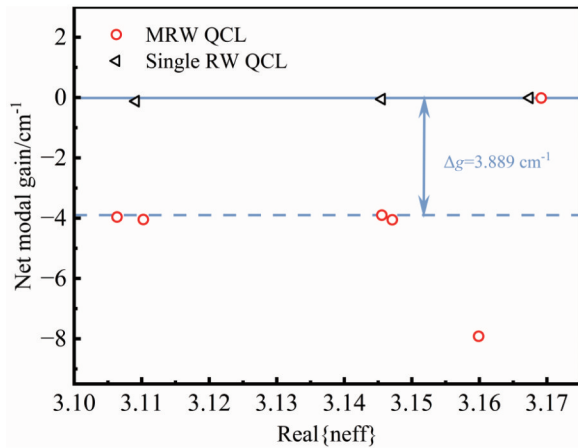


Fig. 9 Mode discrimination of MRW-QCL (red circles) and conventional QCL (black triangles)

图9 MRW-QCL(红心圆)与传统QCL(黑三角)的模式区分能力

single-mode waveguide structure with a  $10\ \mu\text{m}$  ridge width, thereby increasing the active area by 100%, which is of great significance for achieving high power and single transverse mode output of QCL. In future research, we will further consider thermal effects and heat dissipation structure design, study the impact of trench filling on heat dissipation, and strive to achieve wide ridge QCL single-mode output of high-power continuous mode.

## References

- [1] Quach P, Liu S F, Jollivet A, et al. A GaN/AlN quantum cascade detector with a broad response from the Mid-infrared ( $4.1\ \mu\text{m}$ ) to the Visible ( $550\ \text{nm}$ ) Spectral Range [J]. Applied Physics Letters, 2020, 116 (17) :171102.
- [2] Fei T, Zhai S T, Zhang J C, et al. High power  $\lambda \sim 8.5\ \mu\text{m}$  quantum cascade Laser grown by MOCVD operating continuous-wave up to 408 K [J]. Journal of Semiconductors, 2021, 42 (11) :112301.
- [3] Wang Z, Beck M, Wang R, et al. Monolithic integration of mid-infrared quantum cascade lasers and frequency combs with passive waveguides [J]. ACS Photonics, 2022, 9(2):426-431.
- [4] Liu C W, Zhai S Q, Zhang J C, et al. Free-space communication based on quantum cascade laser [J]. Journal of Semiconductors, 2015, 36(9):85-88.
- [5] Figueiredo P, Suttinger M, Go R, et al. Progress in high-power continuous-wave quantum cascade lasers [J]. Applied Optics, 2017, 56 (31):H15.
- [6] Liu Y H, Zhang J C, Yan F L, et al. Coupled ridge waveguide distributed feedback quantum cascade laser arrays [J]. Applied Physics Letters, 2015, 106(14):553.
- [7] Heydari D, Bai Y, Bandyopadhyay N, et al. High brightness angled cavity quantum cascade lasers [J]. Applied Physics Letters, 2015, 106(9):941.
- [8] Yu S, Fang Z, Wang Z Z, et al. On-chip single-mode thin-film Lithium Niobate fabry-perot resonator laser based on sagnac loop reflectors [J]. Optics Letters, 2023, 48(10):2660-2663.
- [9] Praveena S, Senthilnathan K. A review: Rise of pt-symmetry for laser applications [J]. Optik, 2023, 289(17): 171260.
- [10] Song A Y, Kalapala A R K, Gibson R, et al. Controllable finite ultra-narrow quality-factor peak in a perturbed dirac-cone band structure of a photonic crystal slab [J]. Applied Physics Letters, 2021, 119(03):03115.
- [11] Fu T, Wang Y F, Wang X Y, et al. Microstructure lasers based on parity-time symmetry and supersymmetry [J]. Chinese Journal of Lasers, 2021, 48(12):1201005.  
傅廷, 王宇飞, 王学友等. 基于PT对称和超对称的微结构激光器. 中国激光, 2021, 48(12):1201005.
- [12] Hokmabadi M P, Nye N S, El-Ganainy R, et al. Supersymmetric laser arrays [J]. Science, 2019, 363(6427):623-626.
- [13] Qiao X, Midya B, Gao Z, et al. Higher-dimensional supersymmetric microlaser arrays [J]. Science, 2021, 372(6540):403-408.
- [14] Zhao X L, Zeng S, Sweatt L, et al. High-power single-mode triple-ridge waveguide semiconductor laser based on supersymmetry [J]. AIP Advances, 2021, 11(9):095216.
- [15] Hayenga W E, Garcia-Gracia H, Cristobal E S, et al. Electrically pumped microring parity-time-symmetric lasers [J]. Proceedings of the IEEE, 2020, 108 (5) :827-836.
- [16] Abbas M, Ziauddin, Zhang Y C, et al. Phase dependent parity time symmetry in a quantum dot nanostructure [J]. Optics & Laser Technology, 2023, 162 (10):109259.
- [17] Fu T, Wang Y F, Wang X Y, et al. Mode Control of quasi-PT symmetry in laterally multi-mode double ridge semiconductor laser [J]. Chinese Physics Letters, 2020, 37(4):044207.
- [18] Guo A, Salamo G J, Duchesne D, et al. Observation of PT-symmetry breaking in complex optical potentials [J]. Physical Review Letters, 2009, 103(9):093902.
- [19] Gu Z Y, Zhang N, Lyu Q, et al. Experimental demonstration of PT-symmetric stripe lasers [J]. Laser & Photonics Reviews, 2016, 10 (4):588-594.
- [20] Chen Y T, Wang J W, Chen W J, et al. Reciprocal waveguide coupled mode theory [J]. Acta Physica Sinica, 2020, 69 (15) :154206.
- [21] Guan Y J, Lu X Y, Cheng F M, et al. Continuous-wave Distributed Bragg reflector quantum cascade lasers with fine single-mode tuning up to  $102^\circ\text{C}$  at  $\lambda \sim 8.4\ \mu\text{m}$  [J]. Optics Communications, 2023, 528 (12) :128994.
- [22] Yang R K, Zhang D L, Zheng X T, et al. Optics and thermal co-optimal design of high-power quantum cascade lasers [J]. Laser & Infrared, 2023, 53 (9) :1350-1359.  
杨若珂, 张东亮, 郑显通等. 大功率量子级联激光器的光学与热学协同优化设计. 激光与红外, 2023, 53 (9) :1350-1359.